International Journal of Energy for a Clean Environment 22(X):1–18 (2021)

EFFECT OF PORE DIFFUSION ON THE GASIFICATION CHARACTERISTICS OF COAL CHAR UNDER CO_2 ATMOSPHERE

***M. Shahabuddin,*[1,2,*] *M.A. Kibria,*[1] *& Sankar Bhattacharya*[1]**

[1]*Department of Chemical Engineering, Monash University, Wellington Rd., Clayton 3800, Australia*

[2]*Carbon Technology Research Center, School of Engineering, Information Technology and Physical Sciences, Federation University, P.O. Box 3191, Gippsland VIC 3841, Melbourne, Australia*

*Address all correspondence to: M. Shahabuddin, Department of Chemical Engineering, Monash University, Wellington Rd., Clayton 3800, Australia; Carbon Technology Research Center, School of Engineering, Information Technology and Physical Sciences, Federation University, P.O. Box 3191, Gippsland Mail Center, Melbourne, Australia, E-mail: shahabuddin.suzan1@gmail.com

Original Manuscript Submitted: ?/?/2020; Final Draft Received: ?/?/2020

The effect of pore diffusion on kinetic parameters is of particular interest to the current study using coal char under CO_2 gasification conditions. A high-temperature entrained-flow gasifier was used for the preparation of char through the rapid pyrolysis process. The kinetic study with the char was then carried at temperatures of 973–1473 K under atmospheric pressure. A prediction of carbon conversion for large particle size (100 μm) is reported from the carbon conversion of small particle size (25 μm) considering the diffusion effect. The effect of diffusion caused by temperatures and particle size was reported through activation energy. The apparent activation energy in the chemically controlled region (973–1173 K) was calculated to be 178 kJ/mol, whereas it was 69 kJ/mol in the pore diffusion zone (1373–1473 K) using smaller particle size. The apparent activation energy using large particle size was found to be 186 and 99 kJ/mol in chemically controlled and pore diffusion zone, respectively. The intrinsic activation energy for both particle sizes was almost similar. A variation between apparent and intrinsic reaction rates was depicted mostly at higher temperatures of over 1273 K. The change in the surface area of char particle was crucial in terms of decreasing reaction rates, which was decreased with the progression of the conversion. The predicted carbon conversion for large particle size was in good agreement with the experimentally measured conversion except for little discrepancies at higher temperatures.

KEY WORDS: *kinetic study, pore diffusion, coal gasification, activation energy, TGA*

NOMENCLATURE

a.f.b	ash free basis	R_{app}	apparent reaction rate
A_0	pre-exponential factor of the Arrhenius equation	R_{int}	intrinsic reaction rate
		S_0	initial surface area of char
BCMCL	Barapukuria coal mining company limited	S_g	surface area of char at conversion x
D_b	molecular diffusion coefficient	T	temperature
D_{eff}	effective gas diffusion coefficient	TGA	thermogravimetric analyser
D_K	Knudsen diffusion coefficient	w_i	initial weight of the sample
d_p	particle diameter	w_t	weight of the sample at time t
E_a	apparent activation energy	x	carbon conversion
f_c	reaction function		
$K_{D,\,CO_2}$	mass transfer coefficient of CO_2	**Greek Symbols**	
M_1, M_2	molecular weight of carbon and CO_2	ε	particle porosity
		η	overall effectiveness factor
N	reaction order	η_{ex}	external effectiveness factor
P_{CO_2}	partial pressure of CO_2	η_{in}	internal effectiveness factor
$P_{CO_2,\,\infty}$	partial pressure of CO_2 at the ambient atmosphere	ρ_p	particle density
		σ	average collisional diameter
$P_{CO_2,\,s}$	partial pressure of CO_2 surrounding the particle surface	τ	tortuosity factor of the pore
		φ	Thiele modulus
q_{CO_2}	depletion flux of CO_2 due to the reaction	Ψ	char structural parameter for the random pore model
R	universal gas constant	Ω	collisional integral

1. INTRODUCTION

Gasification technology has been used extensively for power generation and chemicals synthesis. The gasification performance using coal is greatly influenced by the reaction rate of coal char (Gilot et al., 2017; Shahabuddin et al., 2020b; Storm et al., 2005) because gasification is a rate-limiting process, associated with multiple complex homogeneous and heterogeneous reactions (Kajitani et al., 2006; Panchuk et al., 2019). Factors affecting gasification rate include temperature, heating rate, operating pressure, reactant types, and the physicochemical properties of feedstocks. Predominantly, kinetic study of gasification has been conducted under a chemically controlled zone at temperatures between 700^{o}C and 900^{o}C (Tanner and Bhattacharya, 2016). It is commonly believed that the kinetic parameter calculated from the chemically controlled zone is capable of describing pore diffusion phenomena happened under high-temperature zone (Ferreira et al., 2020; Kim et al., 2014). However, the optimum experimental conditions to determine kinetic pa-

rameters is controversial in the literature — most of the studies have been conducted within the temperature range of 700–1100^{o}C using a thermogravimetric technique (Huo et al., 2014; Kajitani et al., 2006; Migliavacca et al., 2004; Tanner and Bhattacharya, 2016).

Different research groups have conducted numerous studies to calculate kinetic parameters under CO_2 gasification conditions using different types of coal. Goyal et al. (1989), for example, studied the kinetic parameter for bituminous coal char using different reactants, including CO_2 within the temperature range of 925–1038^{o}C and pressure from 4 to 28 atm. The results showed that the effect of pressure on the gasification rate is negligible, and the developed correlation can predict the gasification rate constant in fluidized bed application. Tanner and Bhattacharya (2016) studied the kinetic parameters for Victorian brown coal in CO_2 and steam atmosphere using different physical models within the temperature range of 650–1100^{o}C. The study of the effect of CO_2 partial pressure on gasification reactivity was also conducted. The results showed that the reaction rate was chemically controlled up to the temperature of 900^{o}C and CO_2 partial pressure had a significant impact on reactivity. Porada et al. (2017) compared the reactivity of parent coal and its char under CO_2 gasification conditions over the temperature range of 850–950^{o}C and the pressure from 0.1 to 1.1 MPa. It was reported that the reactivity of parent coal is much higher than of its char.

Furthermore, the positive effect of system pressure was reported as increasing the operating pressure decreased the activation energy. The reactivity of coal gasification at different stages of conversion was tested using South Australian low-rank coal over the temperature range of 900–950^{o}C and at atmospheric pressure (Poeze and Zhang, 1996). The results showed that the reactivity decreases with the progress of the conversion (Arenillas et al., 2005). The understanding of kinetic parameters under kinetically controlled zone is well developed, whereas only a few studies are available using a temperature range above 1000^{o}C (Roberts et al., 2010; Tremel and Spliethoff, 2013). Studies considering kinetically controlled temperature do not take into account diffusion limitation while calculating kinetic parameters. Therefore, the gasification rate calculated in those studies is associated with some degree of error because of not considering pore diffusion limitation (Huo et al., 2014), especially where the operating conditions (i.e., particle size, flow rate) are not optimized. The practical entrained-flow gasifiers are operated in the tempe ratures range of 1200–1600^{o}C, which is considered to be the pore diffusion-controlled zone (Shahabuddin et al., 2020a,c). Thus, while calculating kinetics parameters, the consideration of both kinetically controlled and diffusion-controlled zones are essential to account for the effect of internal and external pore diffusions (Roberts et al., 2010).

A comparison of kinetic parameters obtained from chemical kinetics and pore diffusion zones has been shown in Roberts et al. (2010). The effect of temperature and CO_2 partial pressure was reported through activation energy and reaction order. The results showed that the activation energy determined under diffusion-controlled zone is markedly lower than that of the pore diffusion zone. Also, in-

creasing the CO_2 partial pressure increases the reaction rate. Apart from temperature and pressure, particle size affects diffusion resistance and subsequently, the gasification rate and carbon conversion (Shahabuddin and Bhattacharya, 2018). Therefore, in this study, a prediction of carbon conversion for large particle size is reported with the help of experimental carbon conversion of small particle size considering diffusion resistance. Limited studies are available in the literature where the pore diffusion effect is considered while determining kinetic parameters. Some studies (Kabir et al., 2016; Tanner and Bhattacharya, 2016) used a smaller particle size to eliminate pore diffusion effect. However, other influential parameters, for example, sample mass, reactant flow rate, and crucible configuration, were not optimized. Some recent studies (Dai et al., 2017; Huo et al., 2014; Kim et al., 2014) showed that the pore diffusion effect is significant, especially at a higher temperature and in the initial stage of conversion. Kim et al. (2014) modeled particle diffusion over the temperature range of 973–1723 K using a thermogravimetric study. It was reported that the pore diffusion effect is relatively low up to the temperature of 1173 K, which is significant at higher temperatures. Huo et al. (2014) showed the pore diffusion effect in terms of effectiveness factor and found that the pore diffusion effect increases with increasing temperature and particle size. Similarly, a study conducted by Dai et al. (2017) stated that the gasification rate is dependent on pore diffusion and decreasing particle size increases the gasification rate considerably.

Different kinetic models have been developed to describe the char gasification behavior. However, every model has some limitations and assumptions. For example, volumetric and grain models assume gas–solid reaction happens uniformly, while there is no consideration for the change in char structure (Levenspiel, 1979). In contrast, the random pore model (RPM) developed by Bhatia and Perlmutter (1980) considered the structural change of particles while determining gasification reactivity. The structural parameter ψ was calculated using experimental data via regression analysis. At diffusion-controlled temperature, surface area, apparent density, and pore diameter (mean free path) of the solid char evolve spontaneously. Also, the gas phase viscosity and diffusivity alter concerning temperatures. In this study, all these changes have been taken into account by internal and external diffusions integrated with RPM. The internal diffusion was calculated via the effectiveness factor as a function of Thiele modulus (Gilot et al., 2017; Kajitani et al., 2006; Kim et al., 2014). The results of this study can be a theoretical basis for the process simulation and will be technically useful, particularly for the industrial-scale gasification.

2. MATERIALS AND METHOD

2.1 Sample Preparation

The char used in this study was prepared from Barapukurian bituminous coal collected from Dinajpur, Bangladesh. The coal sample was crushed, grounded, and sieved to a particle size of 90–106 μm. A high-temperature electrically heated en-

trained-flow gasifier was used to prepare the char through rapid pyrolysis at a temperature of 1200°C under atmospheric pressure. The details of the experimental setup and operating conditions are described in Shahabuddin and Bhattacharya (2019) and Shahabuddin et al. (2020b). The results of proximate and ultimate analyses of the coal and char presented are shown in Table 1.

2.2 Thermogravimetric Analysis

This study used a Netzsch STA 449 F3 thermogravimetric analyser (TGA) for proximate analysis and CO_2 gasification. A 2400 Series II CHNS/O analyser was used for ultimate analysis. The standards used for proximate and ultimate analyses were AS1038.1 (Australian Standard, 2001) and BS ISO 29541-2010, respectively. The gasification studies were conducted at six different temperatures between 700°C and 1200°C with an interval of 100°C under atmospheric pressure. A sample of mass 10 ± 0.5 mg was loaded onto the platinum crucible having a diameter of 18 mm, a length of 2 mm, and a wall thickness of 0.5 mm. A total reactant flow rate of 120 mL/min was used for the CO_2 gasification as an optimized flow rate. The sample was initially heated with a heating rate of 5°C/min up to 105°C and followed by isothermal heating for 20 min to remove moisture present with the presence of N_2. After that, the heating rate was increased to 10°C/min up to the desired reaction temperature. Again, 20-min isothermal heating was set to negate gas switching effect. After that, the N_2 flow was switched to pure CO_2 flow for gasification during 2–3 h. The details of the operating conditions for TGA are outlined in Table 2.

Analogous experiments were carried out using blank crucible for each gasification trial. Data from the blank experiment were then subtracted from the experiment with coal/char sample to negate any bouncy effect, balance drift, and influence of thermal lag between sample and crucible. The crucible was placed on a highly sensitive analytical balance inside the reactor of the TGA. During experiments, this balance can accurately provide weight loss profile over time. The ash-free carbon conversion of char was calculated from the following equation:

TABLE 1: The proximate and ultimate analysis of the coal and char sample

Sample	Moisture	Proximate Analysis (wt.%, air-dry basis)			Ultimate Analysis (wt.%, dry basis)					
		VM	FC	Ash	C	H	N	S	O	Ash
Coal (90–106 μm)	3.10	30.60	57.80	11.60	74.19	4.60	1.52	0.55	7.55	11.60
Char (~100 μm)	1.50	7.11	68.53	24.37	74.28	0.20	1.18	0.30	0.95	23.09
Char (~25 μm)	1.76	8.65	65.59	25.75	—	—	—	—	—	—

TABLE 2: Operating conditions of TGA

Parameters	Value	Parameters	Value
Temperature	700–1200^{o}C	CO_2 concentration	30–90% with N_2
Heating rate	10 K/min	Particle size	~25 and ~100 μm
Pressure	Atm. (101.325 kPa)	Flow rate	120 mL/min
Gasification agents	CO_2	Sample mass	10 mg
Purge gas	pure N_2		

$$x = \frac{w_i - w_t}{w_i}, \tag{1}$$

where x is the carbon conversion, w_i is the initial weight of the sample, and w_t is the weight of the sample at time t.

2.3 Apparent Reaction Rate Modeling

Gasification reaction is a rate-limiting step and to determine the reaction rate, several models have been proposed using either CO_2 or steam as a reactant. The general form of the reaction rate can be written as the time derivative of carbon conversion as follows:

$$R_{\text{app}} = \frac{dx}{dt}. \tag{2}$$

The most simplified reactivity model is the volumetric model, where it is assumed that the gasification reaction takes place uniformly throughout the whole particle. The changes in particle size and structure have been taken into consideration in this model. Whereas, the shrinking core or grain model assumes that the reaction takes place at the outer surface of the particles. The reactant gas progressively diffuses through the core of the particle, which continuously keeps shrinking and forms a new core for the reaction to occur with the reactant. The most developed model considering the change in the particle structure is the RPM, which was developed by Bhatia and Perlmutter (1980). As the reaction of C–CO_2 progresses, the micropores collapse into mesopores, which alters the particle surface area. In the RPM, a structural parameter is considered, which governs the surface area thus resulting in the reaction rate. The change in the surface area due to pore growth can be calculated as (Kajitani et al., 2002)

$$S_g = S_0 (1 - x) \sqrt{1 - \psi \ln (1 - x)}, \tag{3}$$

where S_g is the surface area at conversion x, S_0 is the initial surface area, and ψ is the structural parameter, representing an initial pore structure. The structural pa-

rameter determines the probability of pore growth. The higher value of the structural parameter ψ indicates a greater possibility of pore development (Kim et al., 2014). This structural parameter can be calculated from the pore length L_0, porosity ε, and initial surface area S_0 using the following equation:

$$\psi = \frac{4\pi L_0 (1 - \varepsilon)}{S_0}. \tag{4}$$

However, due to the difficulties of calculating the pore length, it is easier to calculate ψ through the curve fitting in RPM for the apparent reaction rate as (Kajitani et al., 2006)

$$R_{app} = k_p (1 - x) \sqrt{1 - \psi \ln (1 - x)}, \tag{5}$$

where R_{app} is the apparent reaction rate at any conversion, and k_p is the initial measured rate constant ($dx/dt\big|_x = 0$). Experiments were conducted at temperatures of 700–1200°C to calculate those parameters (ψ and k_p), where the gasification rate is controlled by both chemical reaction and pore diffusion (Mann and Kent, 1994; Walker et al., 1959).

2.4 Intrinsic Reaction Rate Analysis

The intrinsic reaction rate was calculated from the *n*th order Arrhenius equation as (Kim et al., 2014)

$$R_{int} = A_0 e^{E_a/RT} (1 - x) P_{CO_2}^n, \tag{6}$$

where A_0 is the pre-exponential factor, E_a is the activation energy, R is the universal gas constant, T is the temperature, x is the conversion, P_{CO_2} is the partial pressure of CO_2, and n is the reaction order. Furthermore, the intrinsic reaction rate can also be determined by the instantaneous surface area during gasification.

2.5 Modeling of External and Internal Diffusion

Beyond chemical kinetics, the reaction rate is controlled by pore diffusion and bulk surface diffusion. In this study, the effect of pore diffusion is modeled, calculating external and internal effectiveness factors. The concept of effectiveness factor was originally derived from the heterogeneous catalytic reaction. However, the difference in the case of char gasification reaction with that of the catalytic reaction is the change in the volume of particles in the gasification reaction, which is unlike to occur in the catalytic reaction (Huo et al., 2014). Therefore, the initial gasification rate is considered to be the representative, where the structures of the char particles are almost identical. The parameters affecting the internal effectiveness factor as a result of diffusion are the particle size and temperature, whereas

the gasification reactant governs the external effectiveness factor. The effectiveness factor is defined as the ratio of the apparent reaction rate to the intrinsic reaction rate. Hence, the apparent reaction rate based on the external and internal diffusions can be written as

$$R_{\text{app}} = \eta_{\text{ex}}\, \eta_{\text{in}}\, R_{\text{int}}\,, \tag{8}$$

where η_{ex} and η_{in} are the external and internal effectiveness factors and R_{int} is the intrinsic reaction rate. Substituting Eq. (6) in Eq. (8) gives the following equation for apparent reaction rate:

$$R_{\text{app}} = \eta_{\text{ex}}\, \eta_{\text{in}}\, A_{\text{int}}\, e^{-E_{\text{a}}/RT}\, (1 - x)\, P_{\text{CO}_2}^{n}\,. \tag{9}$$

The following equation can calculate the external effectiveness factor:

$$\eta_{\text{ex}} = \frac{P_{\text{CO}_2,\, s}}{P_{\text{CO}_2,\, \infty}}\,, \tag{10}$$

where $P_{\text{CO}_2,\, s}$ is the partial pressure of CO_2 surrounding the particle surface, which is also included in the *n*th order reaction rate to calculate the intrinsic reaction rate. The term $P_{\text{CO}_2,\, s}$ is the partial pressure at ambient atmosphere, which can be calculated from the following equation:

$$P_{\text{CO}_2,\, s} = P_{\text{CO}_2,\, \infty} - \frac{q_{\text{CO}_2}}{k_{D,\, \text{CO}_2}}\,, \tag{11}$$

where $P_{\text{CO}_2,\, \infty}$ is the partial pressure of CO_2 at the ambient atmosphere, q_{CO_2} is the depletion flux of CO_2 due to reaction, and $k_{D,\, \text{CO}_2}$ is the mass transfer coefficient of CO_2. The term q_{CO_2} can be calculated from the following equation:

$$q_{\text{CO}_2} = \frac{d_{\text{p}}}{6}\, \rho_p\, R_{\text{app}}\,, \tag{12}$$

where d_{p} and ρ_{p} are the diameter and apparent density of char particle.

The mass transfer coefficient $k_{D,\, \text{CO}_2}$ in Eq. (11) was calculated from the Chapman–Enskong theory as follows (Hirschfelder et al., 1964; Wilke and Lee, 1955):

$$k_{D,\, \text{CO}_2} = \frac{1.858 \times 10^{-3}\, T^{1.5} \sqrt{1/M_1 + 1/M_2}}{P_{\text{atm}}\, \sigma_{12}^2\, \Omega}\,, \tag{13}$$

where M_1 and M_2 are the molecular weight of carbon and CO_2, T is the absolute temperature, P_{atm} is the atmospheric pressure, σ is the average collisional diameter, and Ω is the collisional integral.

The effectiveness factor for internal diffusion was calculated based on the Thiele modulus φ and reaction function f_c as follows:

$$\eta_{in} = f_c \frac{1}{\varphi}\left[\frac{1}{\tanh(3\varphi)} - \frac{1}{3\varphi}\right]. \tag{14}$$

The term f_c can be calculated as

$$f_c = \left[1 + \frac{0.5^{0.5}}{2\varphi^2 + (2\varphi^2)^{-1}}\right]^{0.5(1-n)}, \tag{15}$$

where the Thiele modulus φ is the ratio of the square rate of the reaction rate to the diffusion rate, which can be calculated from the following equation:

$$\varphi = \frac{d_p}{6}\sqrt{\frac{(n+1)(1-x) r_{int} R_u T_p \rho_p P_{CO_2}^{n-1})}{2 M_p D_{eff}}}, \tag{16}$$

where n is the reaction order, D_{eff} is the effective diffusion coefficient, which is composed of Knudsen diffusion D_k and molecular diffusion D_b and can be represented using the following equations:

$$D_{eff}^{-1} = D_k^{-1} + D_b^{-1}, \tag{17}$$

$$D_k = \frac{2r_p}{3}\sqrt{8R_u T / \pi M_{CO_2}}, \tag{18}$$

$$D_b = \frac{\varepsilon}{\tau} D_{CO_2}, \tag{19}$$

where r_p is the porosity ratio, ε is the porosity, and τ is the tortuosity factor of the pore with a value of 1.41 (Laurendeau, 1978). Based on the literature, the diffusion coefficient of CO_2 with char particles can be calculated by the following correlation:

$$D_{CO_2} = 1.67 \times 10^{-5}\left(\frac{T}{298.15}\right)^{1.75}. \tag{20}$$

3. RESULTS AND DISCUSSION

Figure 1 shows the apparent reaction rate with respect to carbon conversion at a temperature of 1100°C. The structural parameter calculated from 100-µm particles was 3.15, whereas it was 3.0 using 25-µm particles. Under both conditions, the apparent reaction rate was increased up to the conversion of about 20%, from where a gradual decline was observed. The modeled apparent reaction rates are in close agreement with the experimental data up to the conversion of about 60%. The discrepancies between the experimental and modelled data in the later part of the conversion indicate that a single structural parameter in the model is not capable of predicting reaction rate throughout the conversion ranges. It can be seen that the reaction rate in the later stage has become slow, which can be interpreted as the morphological change in the particles due to the pore blockage, annealing, and overall reduction of active sites (Tanner and Bhattacharya, 2016). The details of the physical properties of char are illustrated in Table 3.

The change in BET specific surface area with the progress of carbon conversion is presented in Fig. 2 for two different temperatures and particle sizes. The surface area with respect to carbon conversion was calculated using the correlation developed by Bhatia and Perlmutter (1980). As expected, the surface area for the lower particles is relatively higher than that of larger particles. At a particular conver-

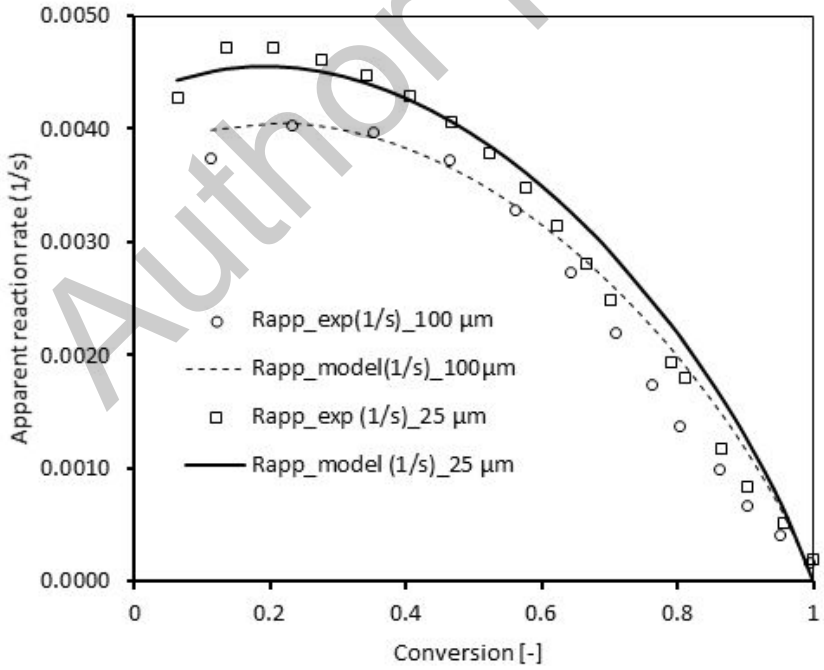

FIG. 1: Apparent reaction rate as a function of char conversion using the RPM at a temperature of 1100°C and atmospheric pressure

TABLE 3: Physical properties of char samples

Properties	~25-μm Particle	~100-μm Particle
Apparent density, g/m^3	1.50	1.60
Initial surface area, m^2/g	94.43	88
Porosity of char particle	0.7	0.7
Pore diameter, μm	3.52	3.97
Pore structural parameter of RPM	3.00	3.15
Reaction order	0.86	1.10

sion, the surface area is found to be different at different operating temperatures. For 100-μm particles, at a conversion of 0.6, the surface area at 900°C was determined to be 82 m^2/g, whereas it was 60 m^2/g at 1000°C. Also, the surface area at higher temperatures is slightly higher up to the conversion of 0.3, which drops gradually with the progression of the conversion.

Furthermore, the difference in surface area from two particle sizes is relatively low at 1000°C compared to the lower temperature of 900°C, especially in the second half of the conversion. The maximum surface area was obtained at a conversion of 21% and 19% for particle size 25 μm ($\psi = 3.0$) and 100 μm ($\psi = 3.15$), respectively. This result is consistent with the results reported in Bhatia and Perlmutter (1980). The current results indicate two critical phenomena. Firstly, the conversion below the maximum conversion represents the growth of reaction surface area, while as the conversion progresses, the pore gradually collapses due to the intersection and loses active surface area for reaction (Walker et al., 1959). Walker and Raats (1956) reported the maximum surface area at a conversion of

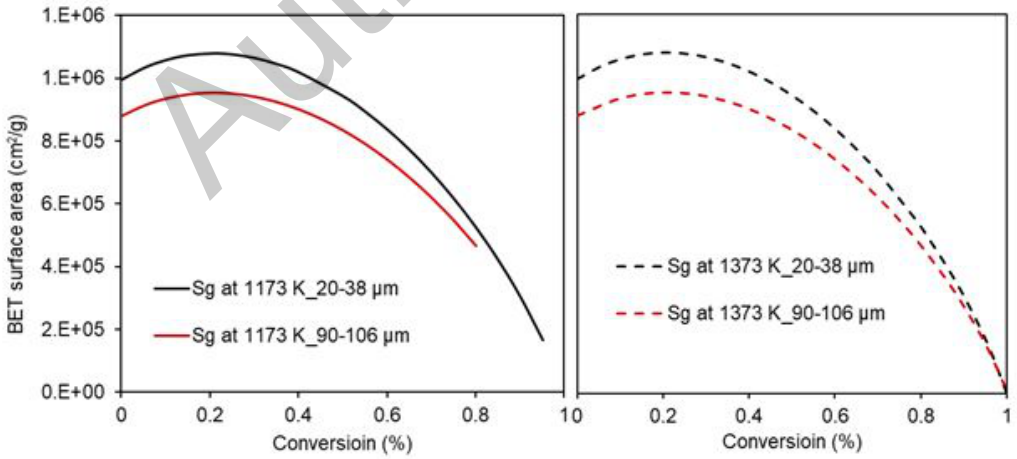

FIG. 2: Change in the surface area for different particle sizes and temperatures concerning char conversion

34.5% for the structural parameter $2 \leq 2\psi < \infty$, while Bhatia and Perlmutter (1980) reported the maximum surface area at a conversion of 39.3%:

$$x_{\max} = 1 - \exp\left[(2 - \psi)\, 2\psi\right] . \tag{21}$$

The intrinsic reaction rate, which is the ratio of the apparent reaction rate to the surface area was further calculated using Eq. (6)

$$R_{\text{in}} = \frac{R_{\text{app}}}{S_g} . \tag{22}$$

The comparison between the apparent and intrinsic reaction rates is plotted in Fig. 3. A significant difference between the apparent and intrinsic reaction rates is observed using both particle sizes. The surface area entirely controls the intrinsic reaction rate; thus, the profile of the intrinsic reaction rate is inversely proportional to the change in the surface area concerning temperature. The variation in reaction rates in the lower temperature zone is relatively low compared to the higher temperature zone.

The kinetic parameters calculated under kinetically and diffusion-controlled regimes are shown in Table 4. The higher activation energy using larger particle size implies that the particles with large size have more prone to exert diffusion resistance. Despite, it can be noticed that the intrinsic activation energy from both par-

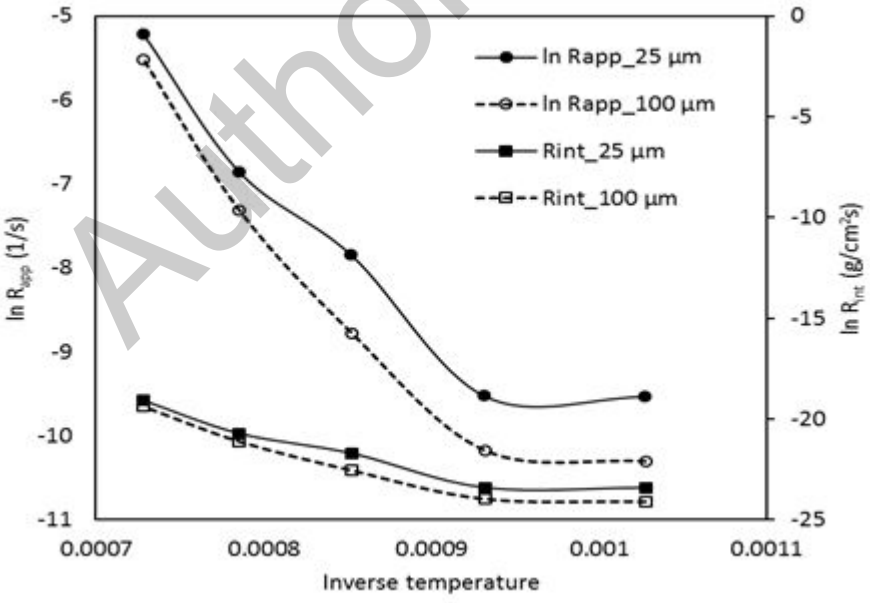

FIG. 3: Comparison between apparent and intrinsic reaction rates with respect to temperatures using different particle sizes

TABLE 4: Kinetics parameters calculated under kinetically and diffusion-controlled regimes

Particle Size, μm	E_{app}, kJ/mol			A_{app}, 1/s			Regime I	
	Regime I	Regime II	Regime I + II	Regime I	Regime II	Regime I + II	E_{in}, kJ/mol	A_{in}, 1/s·atm
20–38	178	69	160	1.2E + 04	2	4.8E + 03	173	1.21E + 04
90–106	186	99	164	2.6E + 03	8	1.9E + 03	176	1.5E + 03

ticle sizes is similar in the kinetically controlled zone, which is 173 kJ/mol and 176 kJ/mol, respectively. The similar activation energies from two different particle sizes confirm the validity of the intrinsic kinetics. The kinetic parameters obtained from this study are in close agreement with the previously calculated kinetic parameters using coal of the same rank (Dai et al., 2017). Furthermore, the data of the pre-exponential factor show that its value for smaller particle size is significantly higher than that for larger particle size. The higher pre-exponential factor for smaller particle size indicates a robust interparticle interaction compared to that of large particle size.

Figure 4 shows the modeled internal effectiveness factor for particle size 90–106 μm. It is worth mentioning that this effectiveness factor was calculated from the experimental data on carbon conversion for smaller particle size at temperatures its 1073 to 1473 K. As seen, increasing the temperature decreases the internal effectiveness factor η_{in}. However, the variation in η_{in} at lower temperatures is not as significant as at higher temperatures, indicating a dominant effect of pore diffusion at higher

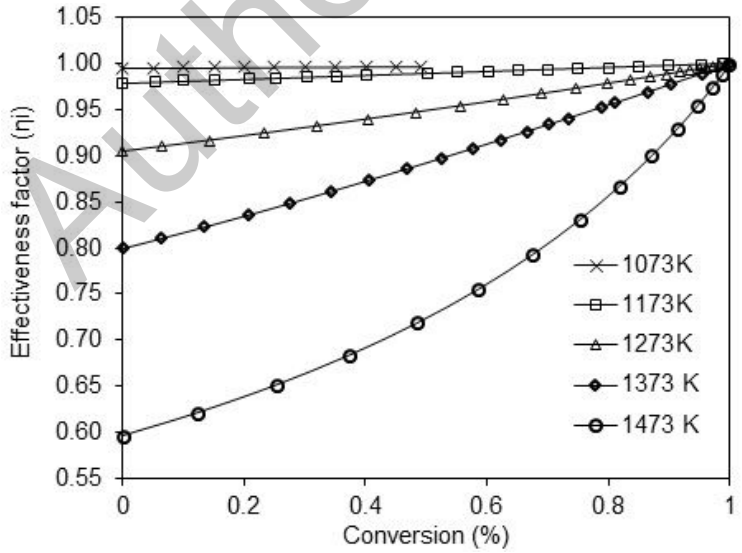

FIG. 4: Internal effectiveness factor for particle size 90–106 μm calculated from the experimental carbon conversion of 20–38-μm particles

temperatures. At lower temperatures, the C–CO_2 reaction is mainly controlled by chemical kinetics, where the pore diffusion limitation is not dominant; thus, the effectiveness factor is close to unity. The profile of the effectiveness factor with respect to conversion shows two distinct features between the temperature ranges of 973–1173 K and 1273–1373 K. In the lower temperature range (regime I), the effectiveness factor shows an almost linear relationship with the conversion. However, the effectiveness factors obtained at higher temperatures (regime II), show an exponentially rise, especially after the conversion of 0.4. The results imply that the pore diffusion effect is dominant in the initial stage of the gasification and decreases with the increasing conversion, as was observed in Huo et al. (2014).

The pore diffusion effect can also be correlated with the Thiele modulus concerning temperature and particle size. Figure 5 shows the variation in the Thiele modulus and average effectiveness factor concerning temperatures. It can be seen that, at all operating temperatures, the effect of pore diffusion is significantly low for 20–38-μm particles compared to that of 90–106-μm particles. The Thiele modulus was increased with increasing temperatures, which is consistent with the results reported in the literature for bituminous coal (Huo et al., 2014).

When the Thiele modulus is less than 0.40, the effect of pore diffusion can be regarded as negligible (Huo et al., 2014). However, when the Thiele modulus is in the range from 0.40 to 3.0, the pore diffusion and chemical reaction jointly control

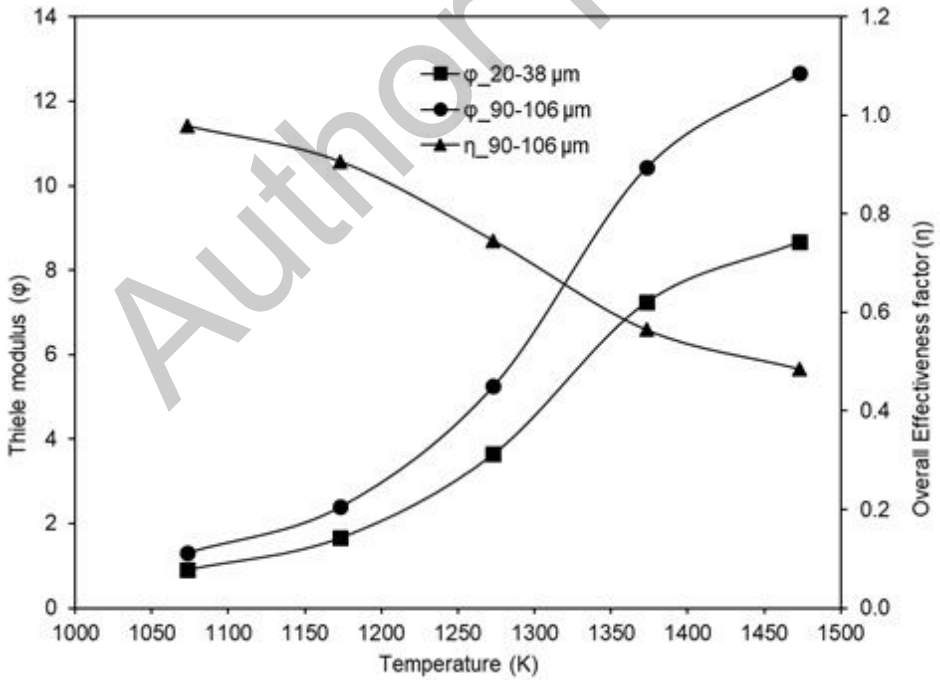

FIG. 5: Effect of temperature and particle size on the Thiele modulus and average effectiveness factor

the reaction rate. Furthermore, the gasification rate is predominantly controlled by pore diffusion when the Thiele modulus is greater than three. The result reveals that the Thiele modulus for both particles is greater than three at a temperature over 1200 K. Also, the Thiele modulus for larger particles is higher than for smaller particles. The results imply that for large particles, the diffusion resistance is more, which takes part in controlling the gasification rate. The change in overall effectiveness factor concerning temperature is also depicted in Fig. 5. Likewise the Thiele modulus, the changes in overall effectiveness factors are low at a lower temperature, whereas the variation is significant at higher temperatures. In the case of smaller particle size, the interparticle diffusion is insignificant, and only the external diffusion contributes to the effectiveness factor, especially at higher temperatures, whereas, for larger particles, both internal and external diffusion effects results in the higher effectiveness factors.

4. MODEL VALIDATIONS

The carbon conversion for 90–106-µm particles was calculated by multiplying the effectiveness factors with the experimental carbon conversion of 20–38-µm particles. For the model validation, CO_2 gasification using 90–106-µm particles was conducted under the operating conditions analogous to those used for 20–38-µm particles. The results presented in Fig. 6 show the comparison between the pre-

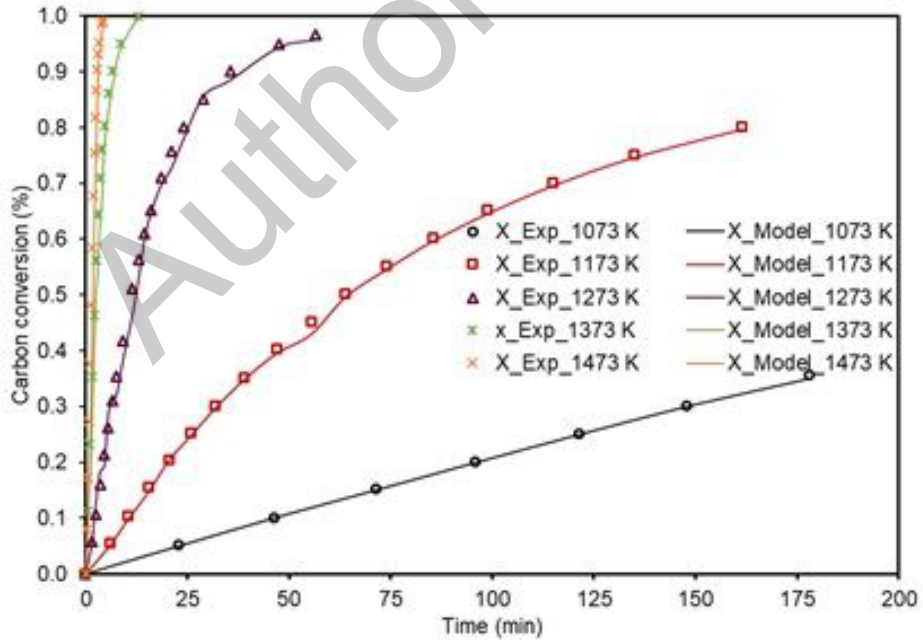

FIG. 6: The prediction of carbon conversion for particle size 90–106 µm with experimental validation

dicted and experimentally measured conversions for particle size 90–106 μm. Good agreement between the experimental and predicted conversions is observed, which confirms the validity of the model.

5. CONCLUSIONS

This study examined the diffusion effect of coal particle size on gasification characteristics and kinetic parameters considering kinetically and diffusion-controlled temperature. It was found that the internal effectiveness factor predicted for a large particle size is dominant at a temperature above 1273 K, while the impact of diffusion is dominant at the initial stage of gasification. The effectiveness factor was only dominant at higher temperatures which increased exponentially with the progression of the conversion. As expected, the effect of pore diffusion was negligible in a lower temperature range. The difference between apparent and intrinsic reaction rates is found to be negligible up to the temperature of 1273 K, above which the difference becomes significant, indicating the effect of temperature on pore diffusion. The model proves that it is possible to predict kinetic parameters and carbon conversion for any particle size and temperature range using a single set of experimental data for a small particle size, where interparticle diffusion is negligible.

REFERENCES

Arenillas, A., Rubiera, F., Moreno, A., Pevida, C., and Pis, J., Study of the Evolution of Nitrogen Compounds during Coal Devolatilization, *Int. J. Energy Clean Environ.*, vol. **6**, no. 4, pp. 393–408, 2005.

Australian Standard Coal and Coke—Analysis and Testing, from https://www.saiglobal.com/PDFTemp/Previews/OSH/as/as1000/1000/1038.16-2005.pdf, 2001.

Bhatia, S.K. and Perlmutter, D.A., Random Pore Model for Fluid–Solid Reactions: I. Isothermal, Kinetic Control, *AIChE J.*, vol. **26** no. 3, pp. 379–386, 1980.

Dai, B., Hoadley, A., and Zhang, L., Characteristics of High Temperature C–CO_2 Gasification Reactivity of Victorian Brown Coal Char and Its Blends with High Ash Fusion Temperature Bituminous Coal, *Fuel*, vol. **202**, pp. 352–365, 2017.

Ferreira, T., Paiva, J., and Pinho, C., Comparative Analysis of Fluidized and Fixed Beds to Obtain Data on the Char Pellet's Combustion Regime, *Int. J. Energy Clean Environ.*, vol. **21**, no. 3, pp. 237–268, 2020.

Gilot, P., Brillard, A., Brilhac, J.-F., and Schönnenbeck, C.A., Simplified Model Accounting for the Combustion of Pulverized Coal Char Particles in a Drop Tube Furnace, *Energy Fuel*, vol. **31**, no. 10, pp. 11391–11403, 2017.

Goyal, A., Zabransky, R.F., and Rehmat, A., Gasification Kinetics of Western Kentucky Bituminous Coal Char, *Ind. Eng. Chem. Res.*, vol. **28**, no. 12, pp. 1767–1778, 1989.

Hirschfelder, J., Bird, R.B., and Curtiss, C.F., *Molecular Theory of Gases and Liquids*, New York, USA: John Wiley & Sons Inc., 1964.

Huo, W., Zhou, Z., Wang, F., Wang, Y., and Yu, G., Experimental Study of Pore Diffusion Effect on Char Gasification with CO_2 and Steam, *Fuel*, vol. **131**, pp. 59–65, 2014.

Kabir, K.B., Tahmasebi, A., Bhattacharya, S., and Yu, J., Intrinsic Kinetics of CO_2 Gasification of a Victorian Coal Char, *J. Therm. Anal. Calorim*., vol. **123**, no. 2, pp. 1685–1694, 2016.

Kajitani, S., Hara, S., and Matsuda, H., Gasification Rate Analysis of Coal Char with a Pressurized Drop Tube Furnace, *Fuel*, vol. **81**, no. 5, pp. 539–546, 2002.

Kajitani, S., Suzuki, N., Ashizawa, M., and Hara, S., CO_2 Gasification Rate Analysis of Coal Char in Entrained Flow Coal Gasifier, *Fuel*, vol. **85**, no. 2, pp. 163–169, 2006.

Kim, R.-G., Hwang, C.-W., and Jeon, C.-H., Kinetics of Coal Char Gasification with CO_2: Impact of Internal/External Diffusion at High Temperature and Elevated Pressure, *Appl. Energy*, vol. **129**, pp. 299–307, 2014.

Laurendeau, N.M., Heterogeneous Kinetics of Coal Char Gasification and Combustion, *Prog. Energy Combust. Sci*., vol. **4**, no. 4, pp. 221–270, 1978.

Levenspiel, O., *Chemical Reaction Engineering*, Chapter 12, New York, USA: John Wiley & Sons Inc., 1979.

Mann, A. and Kent, J.A., Computational Study of Heterogeneous Char Reactions in a Full-Scale Furnace, *Combust. Flame*, vol. **99**, no. 1, pp. 147–156, 1994.

Migliavacca, G., Faravelli, T., Pierucci, S., Ranzi, E., Bonfanti, L., and Parodi, E.A., General and New Kinetic Model of Coal Devolatilization, *Int. J. Energy Clean. Environ*., vol. **5**, no. 3, 2004. DOI: 10/1615/IntJEnerCleanEnv.v5.i3.20

Panchuk, M., Kryshtopa, S., Panchuk, A., Kryshtopa, L., Dolishnii, B., Mandryk, I., and Sladkowski, A., Perspectives for Developing and Using the Torrefaction Technology in Ukraine, *Int. J. Energy Clean. Environ*., vol. **20**, no. 2, pp. 113–134, 2019.

Poeze, A. and Zhang, D. The Effect of Conversion Level on the Gasification Kinetics of a Low-rank Coal [Internet], in G. Weiss, Ed., *Chemeca 96: Excellence in Chemical Engineering; 24th Australian and New Zealand Chemical Engineering Conf. and Exhibition*, Proceedings, Barton, ACT: Institution of Engineers, Australia, 1996, pp. 113–118 [in volume 3], National Cconference Publication (Institution of Engineers, Australia), no. 96/13, cited Oct. 6, 2020, from https://search.informit.com.au/documentSummary;dn=895574537301629;res=IELENG ISBN: 0858256584, 1996.

Porada, S., Czerski, G., Grzywacz, P., Makowska, D., and Dziok, T., Comparison of the Gasification of Coals and Their Chars with CO_2 Based on the Formation Kinetics of Gaseous Products, *Thermochim Acta*, vol. **653**, pp. 97–105, 2017.

Roberts, D.G., Hodge, E.M., Harris, D.J., and Stubington, J.F., Kinetics of Char Gasification with CO_2 under Regime II Conditions: Effects of Temperature, Reactant, and Total Pressure, *Energy Fuel*, vol. **24**, no. 10, pp. 5300–5308, 2010.

Shahabuddin, M., Alam, M.T., Krishna, B.B., Bhaskar, T., and Perkins, G., A Review of Producing Renewable Aviation Fuels from the Gasification of Biomass and Residual Wastes, *Bioresour Technol*., vol. **312**, p. 123596, 2020a.

Shahabuddin, M. and Bhattacharya, S., Gasification Characteristics of Bangladeshi Barapukurian coal in a High-Temperature Entrained Flow Gasifier under CO_2 atmosphereáá Paper presented at the AIP Conf.,ÊÓÐÑÈÂ 8--12 July, Grenoble, France, 2019.

Shahabuddin, M. and Bhattacharya, S., Production of Syngas Using Entrained Flow Gasification of Pine Bark Biomass Aiming to Reduce Greenhouse Gas Emission from Power Generation, Paper presented at the *Int. Conf. on Mechanical, Industrial and Energy Engineering 2018*, 23–24 December, Khulna, Bangladesh, 2018.

Shahabuddin, M., Kibria, M.A., and Bhattacharya, S., Evaluation of High-Temperature Pyrolysis and CO_2 Gasification Performance of Bituminous Coal in an Entrained Flow Gasifier, *J. Energy Inst.*, in press, 2020b.

Shahabuddin, M., Krishna, B.B., Bhaskar, T., and Perkins, G., Advances in the Thermo-Chemical Production of Hydrogen from Biomass and Residual Wastes: Summary of Recent Techno-Economic Analyses, *Bioresour. Technol.*, vol. **299**, p. 122557, 2020c.

Storm, C., Spliethoff, H., and Hein, K.R., Generation of a Gaseous Fuel by Pyrolysis of Biomass and Sewage Sludge for Use as Reburn Gas in Coal-Fired Boilers, *Int. J. Energy Clean Environ.*, vol. **6**, no. 3, pp. 289–328, 2005.

Tanner, J. and Bhattacharya, S., Kinetics of CO_2 and Steam Gasification of Victorian Brown Coal Chars, *Chem. Eng. J.*, vol. **285**, pp. 331–340, 2016.

Tremel, A. and Spliethoff, H., Gasification Kinetics during Entrained Flow Gasification–Part III: Modelling and Optimisation of Entrained Flow Gasifiers, *Fuel*, vol. **107**, pp. 170–182, 2013.

Walker, J. and Raats, E., Changes in Physical Properties of Graphitized Carbon Rods upon Gasification with Carbon Dioxide, *J. Phys. Chem.*, vol. **60**, no. 3, pp. 364–369, 1956.

Walker, P.L., Rusinko, F., and Austin, L., Gas Reactions of Carbon, *Adv. Catal.*, vol. **11**, pp. 133–221, 1959.

Wilke, C. and Lee, C., Estimation of Diffusion Coefficients for Gases and Vapors, *Ind. Eng. Chem.*, vol. **47**, no. 6, pp. 1253–1257, 1955.